Convergent-close-coupling calculations for excitation and ionization processes of electron-hydrogen collisions in Debye plasmas

Mark C. Zammit,* Dmitry V. Fursa, and Igor Bray
Australian Research Council Centre for Antimatter-Matter Studies, Curtin University of Technology, GPO Box U1987, Perth, Western Australia 6845, Australia
(Received 25 June 2010; published 16 November 2010)

Electron-hydrogen scattering in weakly coupled hot-dense plasmas has been investigated using the convergent-close-coupling method. The Yukawa-type Debye-Hückel potential has been used to describe the plasma screening effects. The target structure, excitation dynamics, and ionization process change dramatically as the screening is increased. Excitation cross sections for the $1s \rightarrow 2s,2p,3s,3p,3d$ and $2s \rightarrow 2p,3s,3p,3d$ transitions and total and total ionization cross sections for the scattering from the $1s$ and $2s$ states are presented. Calculations cover the energy range from thresholds to high energies (250 eV) for various Debye lengths. We find that as the screening increases, the excitation and total cross sections decrease, while the total ionization cross sections increase.

DOI: 10.1103/PhysRevA.82.052705 PACS number(s): 34.80.Dp, 34.50.Fa, 52.20.Fs

I. INTRODUCTION

With the advancement of experimental technologies, the past decade has seen an increased interest in the study of hot-dense plasmas [1–8]. These studies have mainly concentrated on the research of inertial confinement fusion, laser-produced plasmas, astrophysics, spectroscopy, plasma, and atomic physics. For hot-dense plasmas that are not in local thermodynamic equilibrium it is important to study the ionization and excitation processes that are used in the determination of ion stage abundance, radiative power losses, and the identification of plasma temperature and pressure. Such plasmas exhibit Coulomb screened interactions, which is a collective, many-particle effect. In the approximation of pairwise correlations, this interaction reduces to the Debye-Hückel potential in weakly coupled plasmas [9]. The Debye-Hückel potential of an ion of positive charge Z that interacts with an electron is given by

$$V(r) = -\frac{Ze^2}{r}\exp\left(-\frac{r}{D}\right), \tag{1}$$

where D is the Debye screening length $D = \sqrt{k_B T_e/4\pi e^2 n_e}$, k_B is the Boltzmann constant, T_e is the electron temperature, and n_e is the electron density. The interaction potential given by (1) is accurate if the Coulomb coupling parameter Γ and nonideality parameter γ are such that $\Gamma \leqslant 1$ and $\gamma \ll 1$, where $\Gamma = e^2/ak_BT_e$, with $a = (3/4\pi n_e)^{1/3}$ being the average interparticle distance, and $\gamma = e^2/Dk_BT_e$.

Several theoretical investigations have been conducted on electron scattering in the Debye plasma environment. It has been shown that the Debye-Hückel potential (1) critically affects the electron scattering processes by changing the target spectrum and excitation dynamics [10–18]. Such studies have mainly concentrated on hydrogenlike targets for low or high incident-electron energies. Kar and Ho [19–21] have investigated several resonance states of the H^- ion interacting with a screened Coulomb (Yukawa) potential using the stabilization method. Recently, Zhang *et al.* [10,11] described low-energy electron-hydrogen scattering using the R-matrix method, concentrating on Feshbach resonances near the $n = 2$ excitation threshold region. High-energy electron-hydrogen excitation processes have been investigated by Qi *et al.* [16] and Hatton *et al.* [17] using the first Born approximation (FBA). The ionization process for electron-hydrogen scattering has been studied by Jung and Joon [18] using a semiclassical approach. However, to date, no study has been conducted on electron-hydrogen excitation and ionization processes in hot-dense weakly coupled (Debye) plasmas over a complete range of energies and Debye lengths. The purpose of the present study is to investigate the effects of a Debye plasma environment on the electron-hydrogen excitation and ionization collision processes across a broad range of incident-electron energies and a wide range of Debye lengths using the convergent-close-coupling (CCC) method [22–25].

This paper is structured as follows. Section II describes the changes made to the CCC theory to include the Debye-Hückel potential (1). Results of our calculations are presented in Sec. III for the target structure and for the various cross sections (CS): integrated, total ionization (TICS), and total cross sections (TCS). The conclusion is given in Sec. IV. Atomic units are used throughout, unless specified otherwise.

II. METHOD

The CCC method for electron scattering on hydrogen atoms has been discussed in detail by Bray and Stelbovics [23]. Briefly, the Sturmian (Laguerre) basis is used to diagonalize the hydrogen atom Hamiltonian under Debye screening:

$$H_T = -\frac{1}{2}\nabla_1^2 - \frac{1}{r_1}\exp\left(-\frac{r_1}{D}\right). \tag{2}$$

This results in a set of N positive- and negative-energy square-integrable pseudostates $\phi_n^{(N)}(r;D)$:

$$\left\langle \phi_f^{(N)}(r;D)\middle| H_T \middle|\phi_i^{(N)}(r;D)\right\rangle = \varepsilon_f^{(N)}\delta_{fi}. \tag{3}$$

With increasing N the negative-energy pseudostates converge to true eigenstates, and the positive-energy states provide an increasingly dense discretization of the continuum. For the Coulomb potential diagonalization in a Sturmian basis

*mark.zammit@student.curtin.edu.au

allows us to represent the infinite number of discrete spectrum states and the continuum via a finite number of pseudostates, which makes subsequent scattering calculations feasible. In the case of the screened Coulomb potential the discrete spectrum contains a finite number of states, which substantially changes the character of the problem from the pure Coulomb case.

The set of pseudostates is then used to perform an expansion of the total wave function for the electron-hydrogen scattering system and formulate a set of close-coupling equations for the T matrix [23]. The CCC method solves the close-coupling equations in momentum space and uses the calculated T matrix to determine cross sections and other observables of interest.

Relatively minor modifications to the CCC method are required in order to describe electron-hydrogen scattering in Debye plasmas. The electron-hydrogen Hamiltonian under Debye screening has the form

$$H = -\frac{1}{2}\nabla_1^2 - \frac{1}{r_1}\exp\left(-\frac{r_1}{D}\right) - \frac{1}{2}\nabla_2^2 - \frac{1}{r_2}\exp\left(-\frac{r_2}{D}\right) + \frac{1}{|r_1 - r_2|}\exp\left(-\frac{|r_1 - r_2|}{D}\right), \quad (4)$$

where r_1 is the distance of the bound electron and r_2 is the distance of the projectile electron to the atom. The account of the electron-nuclei potential (1) is straightforward. The electron-electron potential V_{12} is represented in partial-wave form:

$$V_{12} = \frac{1}{|r_1 - r_2|}\exp\left(-\frac{|r_1 - r_2|}{D}\right) = -\frac{1}{D}\sum_{l=0}^{\infty}(2l+1)\, j_l\left(\frac{ir_<}{D}\right) h_l^{(1)}\left(\frac{ir_>}{D}\right) P_l\cos(\theta). \quad (5)$$

For the unscreened Coulomb case ($D \to \infty$) it reduces to the well-known expression

$$V_{12} = \frac{1}{|r_1 - r_2|} = \sum_{l=0}^{\infty}\frac{r_<^l}{r_>^{l+1}} P_l\cos(\theta). \quad (6)$$

Here $r_< = \min(r_1, r_2)$, $r_> = \max(r_1, r_2)$, and P_l, j_l, and $h_l^{(1)}$ are the Legendre polynomial, spherical Bessel, and Hankel functions of the first kind, respectively. To accurately calculate j_l and $h_l^{(1)}$ with complex arguments the subroutine COULCC of Thompson and Barnett [26] was used. By making the simple substitutions of (1) and (5) in place of the unscreened Coulomb potential the CCC method formulation presented in Ref. [23] remains valid for electron scattering in Debye plasmas.

The CCC method uses the analytical Born subtraction technique to speed up the convergence of the partial-wave expansion. We therefore need to modify for the FBA matrix elements for inelastic scattering. For screened Coulomb potential it is given by

$$\left\langle k_f\phi_f^{(N)}(r;D)\middle|V_{12}\middle|k_i\phi_i^{(N)}(r;D)\right\rangle = \left(\frac{1}{2\pi}\right)^{(3/2)}\frac{1}{D^{-2} + (\vec{k}_f - \vec{k}_i)^2}\int \phi_f^{*(N)}(r;D) \times \exp[i(\vec{k}_f - \vec{k}_i)\cdot r_1]\,\phi_i^{(N)}(r;D)\, d^3r_1. \quad (7)$$

TABLE I. Bound states and pseudostates for various Debye lengths D.

D (units of a_0)	Basis
∞	29 bound states ($1s$–$8s$, $2p$–$9p$, $3d$–$9d$, and $4f$–$9f$) plus 69 pseudostates
20	9 bound states ($1s$–$4s$, $2p$–$4p$, $3d$, and $4d$) plus 89 pseudostates
10	5 bound states ($1s$–$3s$, $2p$, and $3p$) plus 93 pseudostates
4	2 bound states ($1s$ and $2s$) plus 96 pseudostates

III. RESULTS

A. Target structure

We performed diagonalization of the hydrogen atom Hamiltonian for s, p, d, and f states for a number of Debye lengths. A Laguerre basis with an exponential cutoff parameter $\lambda_l = 2$ and basis $N_l = 26 - l$ for $l \leqslant l_{\max} = 3$ has been used. This leads to a total of 98 states. For the Coulomb potential 29 of these states have negative energy (representing hydrogen bound states, $1s$–$8s$, $2p$–$9p$, $3d$–$9d$, and $4f$–$9f$), with the rest providing square-integrable discretization of the target continuum. For incident-electron energies $E \leqslant 20$ eV, only open channels were included; for $E > 20$ eV, the highest-energy s, p, d, and f states were excluded.

It is well known that the screened Coulomb potential (1) supports only a finite number of bound states. This is particularly beneficial for the target atom description in the CCC method as we can obtain accurate representation of most or (depending on the Debye length) all of the bound states. The calculated energies of the bound states are in good agreement with the results presented in Table I by Qi *et al.* [16] and Rogers *et al.* [13], both obtained by a direct numerical solution.

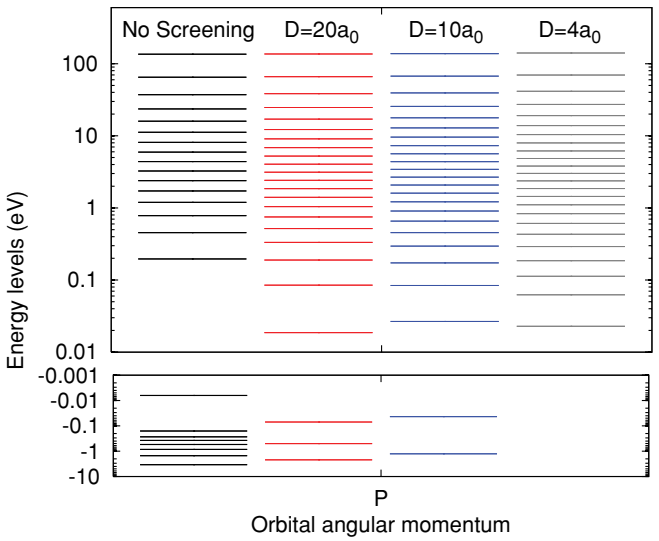

FIG. 1. (Color online) Hydrogen atom spectrum for $l = 1$ for various Debye lengths obtained via diagonalization with $E > 20$ eV scattering Laguerre basis.

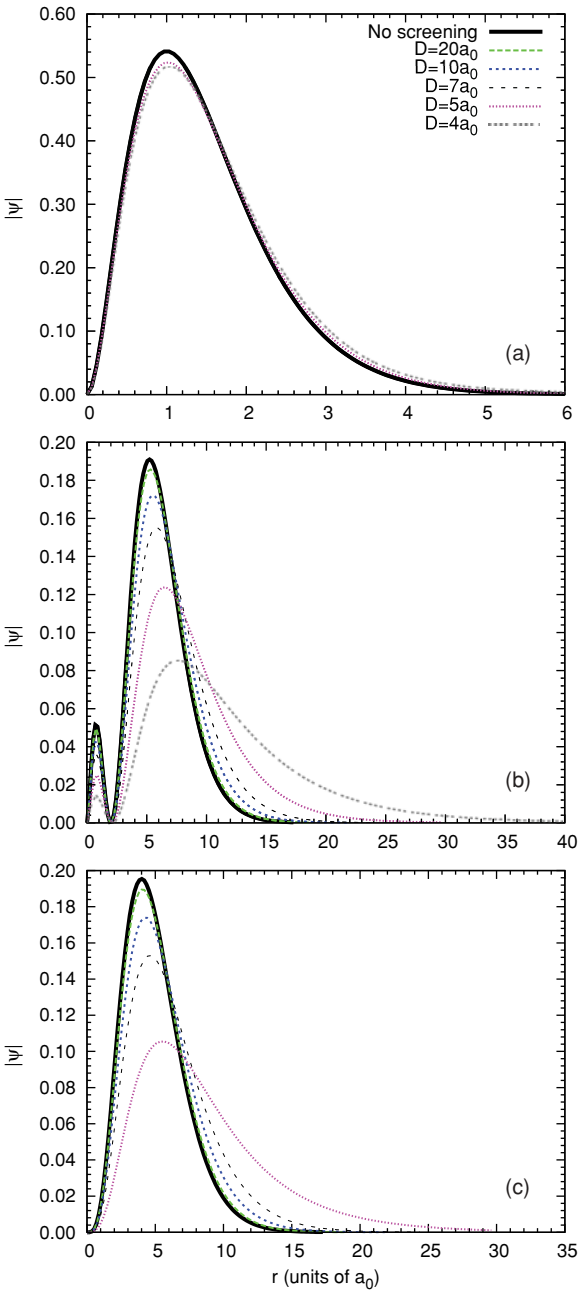

FIG. 2. (Color online) Normalized wave functions $|\Psi|^2$ for the (a) $1s$, (b) $2s$, and $2p$ states.

With a decrease of Debye length the bound state energies increase, which results in a transition of bound states into the continuum. Table I presents results of the number of bound states and pseudostates for the hydrogen atom diagonalized with 98 Laguerre basis functions for several Debye lengths. This is also illustrated in Fig. 1, where we present results of the diagonalization for the hydrogen atom p states for a number of Debye lengths. For example, the $2p$ state merges into the continuum at the critical Debye length $D_c = 4.5a_0$. It can be seen from Fig. 1 that the density of the pseudostates with small positive-energy increases with a decrease of Debye length.

Wave functions for the $1s$, $2s$, and $2p$ states are presented in Figs. 2(a), 2(b), and 2(c), respectively, for various Debye

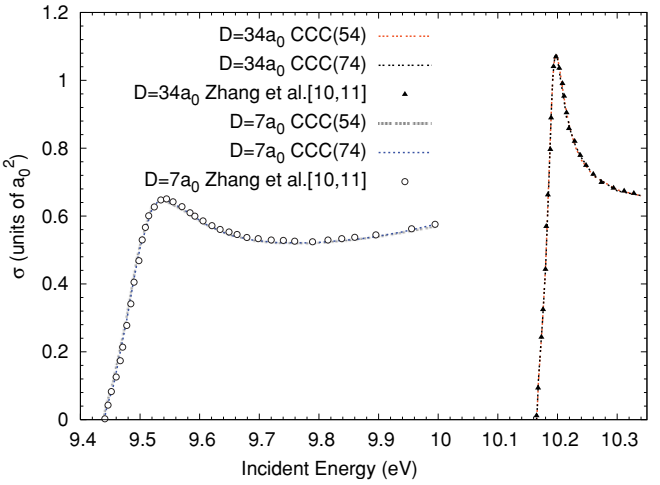

FIG. 3. (Color online) Integrated CS for the $1s \rightarrow 2p$ transition for the $D = 34a_0$ and $D = 7a_0$ screened cases, compared with the results of Zhang *et al.* [10,11].

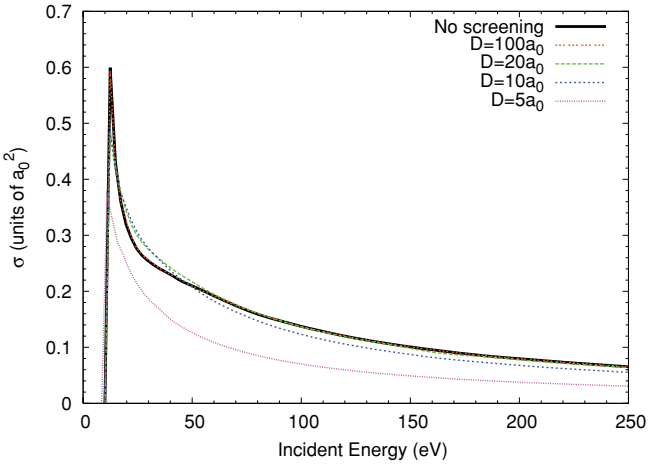

FIG. 4. (Color online) Integrated CS for the $1s \rightarrow 2s$ transition for the Coulomb and screened cases under various Debye lengths.

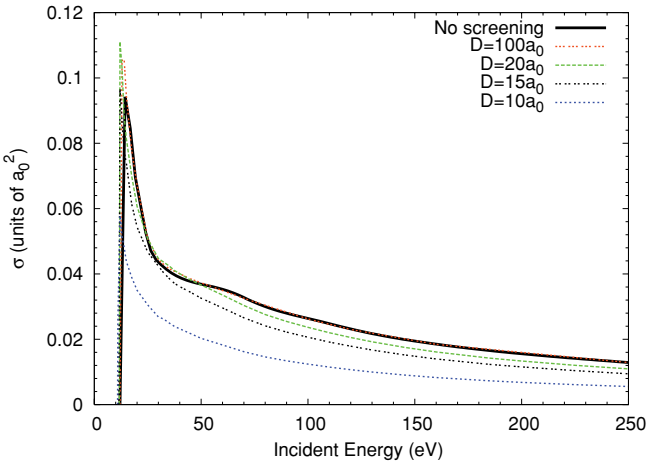

FIG. 5. (Color online) Integrated CS for the $1s \rightarrow 3s$ transition for the Coulomb and screened cases under various Debye lengths.

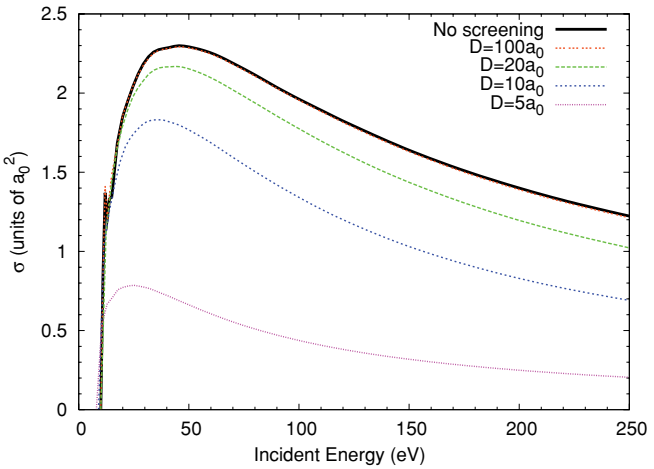

FIG. 6. (Color online) Integrated CS for the $1s \rightarrow 2p$ transition for the Coulomb and screened cases under various Debye lengths.

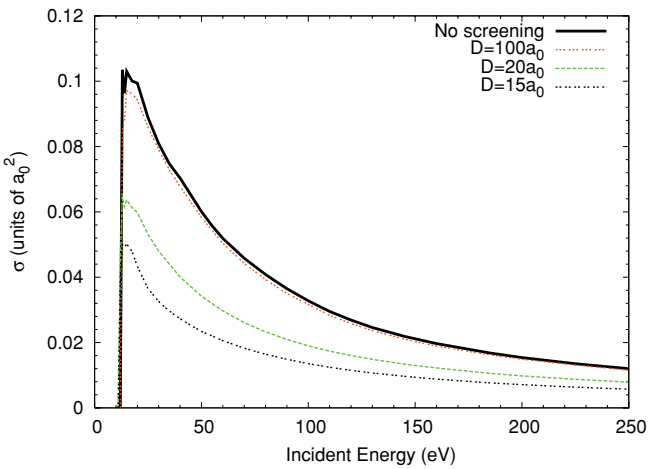

FIG. 8. (Color online) Integrated CS for the $1s \rightarrow 3d$ transition for the Coulomb and screened cases under various Debye lengths.

lengths. With decrease of Debye length the target wave function peaks decrease, broaden, and become more diffuse. The excited states are affected by the Debye screening much more than the ground state. This is expected as the screening modifies Coulomb potential more at larger distances, affecting to a larger degree the more-wide-ranging wave functions.

B. Scattering results

We have performed CCC calculations over a wide range of energies (1–250 eV) and Debye lengths ($D \geqslant 4a_0$). Around 30 partial waves were required to obtain convergence at the largest considered energy. Convergence was tested and verified at selected energies with a basis size of $N_l = 26 - l$ for $l_{\max} = 2$ and $l_{\max} = 4$. Convergence for the Coulomb case was demonstrated by Bray and Stelbovics [23,24], who preformed smaller calculations than those used here.

We have compared our results with Zhang *et al.* [10,11] for transitions at the low-energy resonance region. In Fig. 3 we present the $1s \rightarrow 2p$ transition for $D = 34a_0$ and $D = 7a_0$ near the $n = 2$ threshold region. A basis of $N_l = 15 - l$ and $N_l = 20 - l$ for $l_{\max} = 3$ was used to demonstrate convergence of our calculations. Our results are in good agreement with the relatively small-size R-matrix calculations for both the Debye-Hückel potential and the Coulomb case [27]. This suggests that including a large number of pseudostates is not required to achieve convergence at the low-energy resonance region. We will concentrate here on the cross-section behavior outside the resonance region.

The Debye length dependence of the integrated CS for excitation of the $2s$, $2p$, $3s$, $3p$, and $3d$ states from the ground state and the excitation of $2p$, $3s$, $3p$, and $3d$ from $2s$ together with TICS of the $1s$ and $2s$ states are presented in this section. We find that cross sections for the Debye length $D = 100a_0$ are practically the same as for the Coulomb (no screening) potential. We therefore restrict calculations to $D \leqslant 100a_0$ for all transitions considered in this paper. The present results as well as results for many more transitions will be made available via the CCC database [28].

1. Excitation cross sections

Integrated CS for the $1s \rightarrow 2s$ transitions for various Debye lengths are presented in Fig. 4. We find that generally the

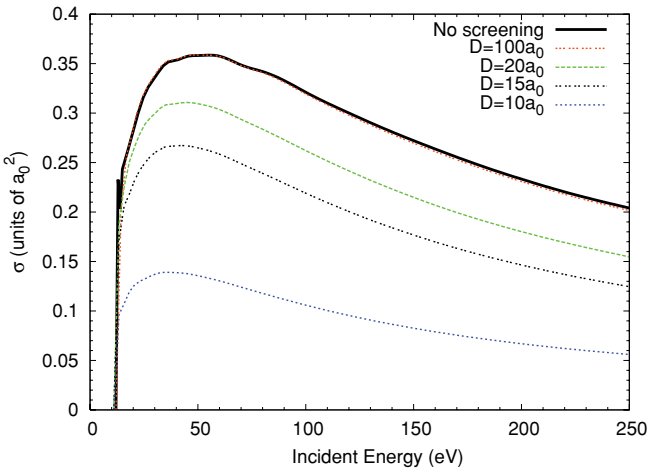

FIG. 7. (Color online) Integrated CS for the $1s \rightarrow 3p$ transition for the Coulomb and screened cases under various Debye lengths.

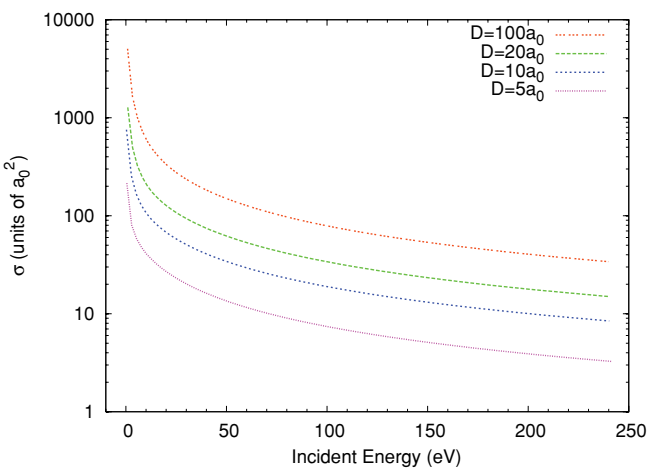

FIG. 9. (Color online) Integrated CS for the $2s \rightarrow 2p$ transition for the screened case under various Debye lengths.

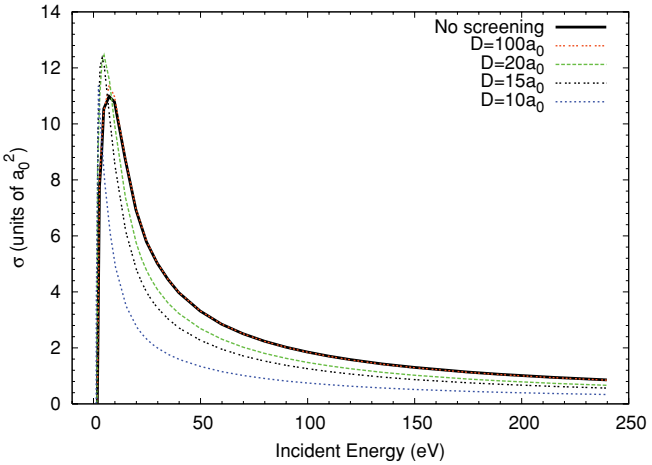

FIG. 10. (Color online) Integrated CS for the $2s \rightarrow 3s$ transition for the Coulomb and screened cases under various Debye lengths.

integrated CS decreases with a decrease of Debye length. The sharp rise of the $1s \rightarrow 2s$ integrated CS at the threshold is present for all Debye lengths; however, with reduction of the Debye length the cross-section maximum becomes smaller and it broadens. From threshold to intermediate energies (∼8–55 eV) we can see nonmonotonic behavior of the integrated CS with change of Debye length ($D > 10a_0$). This is a result of the interplay of reduction of the cross-section maximum and broadening of the cross section as the Debye length decreases. Similar properties are also present in the $1s \rightarrow 3s$ transition, presented in Fig. 5.

Figures 6 and 7 present our results for the $1s \rightarrow 2p$ and $1s \rightarrow 3p$ optically allowed transitions. We find that for both transitions the integrated CS decreases and its peak shifts toward lower energies as the Debye length is decreased. The reduction of the cross section is practically uniform across all energies except for the small, close-to-the-threshold energy region. In the latter region the reduction of the $1s \rightarrow 2p,3p$ excitation energies with decrease of Debye length leads to nonmonotonic behavior.

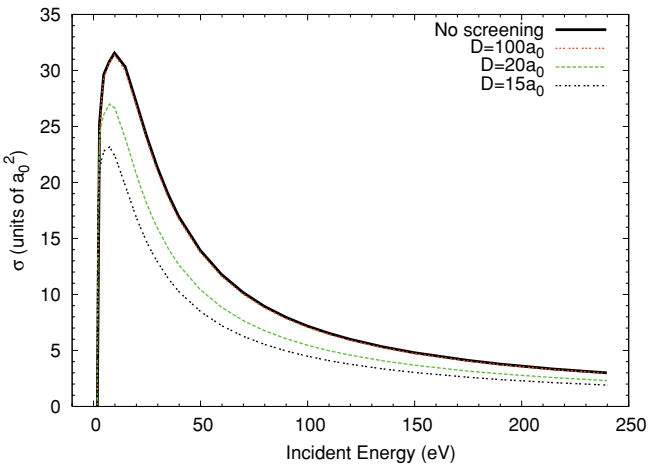

FIG. 11. (Color online) Integrated CS for the $2s \rightarrow 3d$ transition for the Coulomb and screened cases under various Debye lengths.

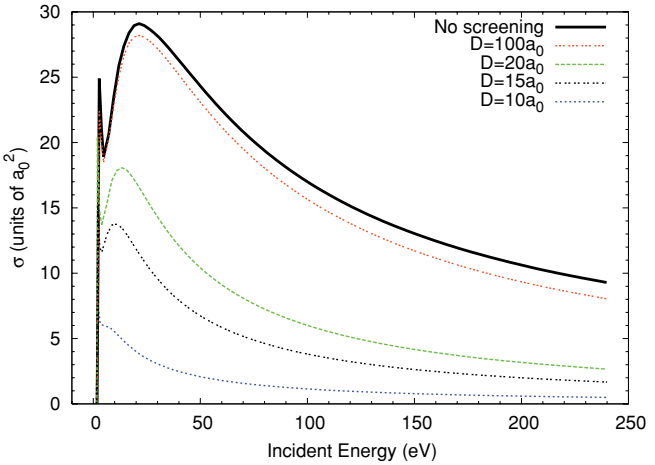

FIG. 12. (Color online) Integrated CS for the $2s \rightarrow 3p$ transition for the Coulomb and screened cases under various Debye lengths.

For the $1s \rightarrow 3d$ transition, presented in Fig. 8, we find uniform reduction of the integrated CS as the Debye length is decreased.

In Fig. 9 we present the $2s \rightarrow 2p$ transition. For the unscreened case, the integrated CS for this transition is infinite due to the degeneracy of the hydrogen atom's energy levels. Debye screening eliminates the degeneracy of the hydrogen atom bound states with the same principle quantum number. This leads to finite excitation cross sections. Figure 9 shows

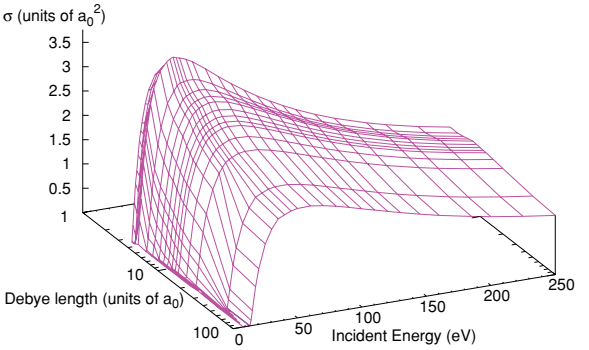

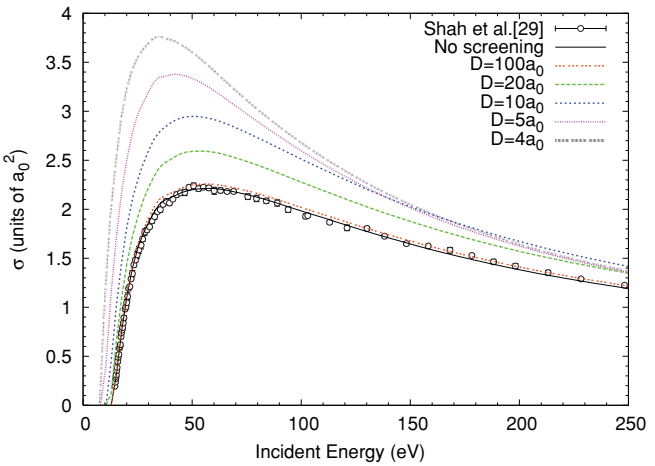

FIG. 13. (Color online) TICS for the $1s$ state for the Coulomb and screened cases under various Debye lengths. The measurements of Shah *et al.* [29] are compared with the Coulomb case.

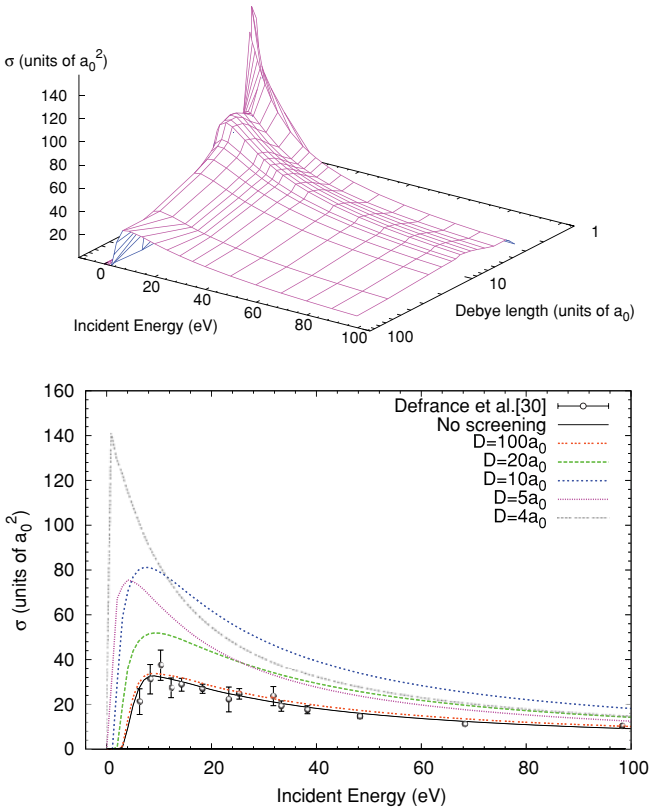

FIG. 14. (Color online) TICS for the $2s$ state for the Coulomb and screened cases under various Debye lengths. The measurements of Defrance *et al.* [30] are compared with the Coulomb case.

the uniform reduction of the $2s \rightarrow 2p$ integrated CS with a decrease of Debye length.

The behavior of the cross sections for optically prohibited $2s \rightarrow 3s,3d$ transitions, presented in Figs. 10 and 11, and optically allowed $2s \rightarrow 3p$ transition, presented in Fig. 12, is very similar to the corresponding ground state excitation cross sections.

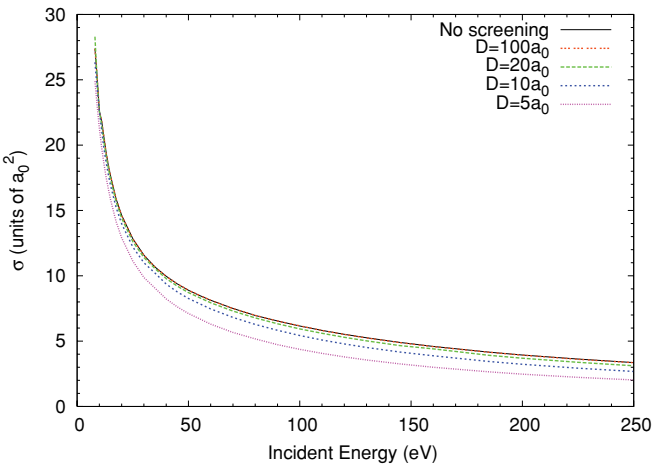

FIG. 15. (Color online) TCS for the $1s$ state for the Coulomb and screened cases under various Debye lengths.

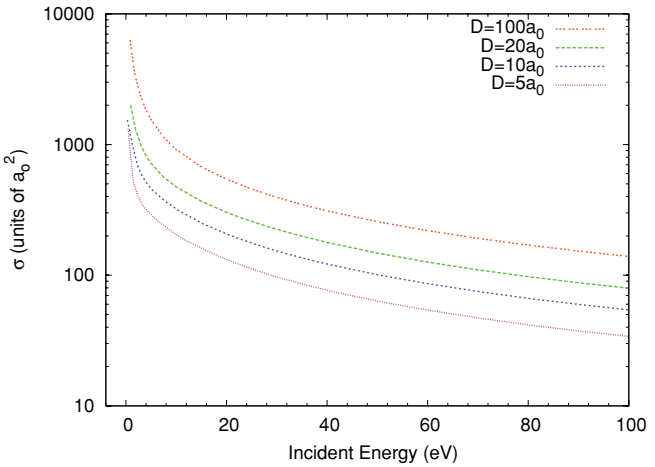

FIG. 16. (Color online) TCS for the $2s$ state for the screened case under various Debye lengths.

2. *Total and total ionization cross sections*

The ground state TICS are presented in Fig. 13. For the Coulomb case our results are in excellent agreement with the experimental data of Shah *et al.* [29]. As Debye length decreases, the TICS becomes larger, and its peak shifts to lower energies. This is due to a combination of an increase in the number of states merged into the continuum and the decrease in the ionization energy of the ground state. In particular, at Debye length $D < 0.85a_0$ all excited states of the hydrogen atom merge into the continuum. Note that behavior of TICS with change of Debye length is opposite to the behavior of excitation cross sections. In the CCC method the TICS is calculated as a sum over integrated CS for all positive-energy states. This means that with decrease of Debye length D the TICS is constructed from an increasing number of positive-energy-state integrated CS, which individually decrease in value. When, with decrease of Debye length D, all discrete spectrum states merge into the continuum ($2p$ state at $D_c = 4.5a_0$ and $2s$ state at $D_c = 3.2a_0$), any further decrease of Debye length will lead to a corresponding decrease of the TICS.

For the metastable $2s$ state TICS are presented in Fig. 14. Similar to the scattering from the ground state, the TICS of the $2s$ state increases with a decrease of Debye length. For the Coulomb case our results are in good agreement with the experimental data of Defrance *et al.* [30]. The TICS peak shifts to lower energies with decrease of Debye length, and monotonic behavior is observed across a whole range of energies. The sharp rise in the TICS when Debye length D decreases from $5a_0$ to $4a_0$ is primarily due to the transition of the $2p$ state into the continuum.

The reduction of projectile-target interaction as Debye screening increases (reduction of Debye length D) should lead to a reduction of the total scattering cross section. This is, indeed, the case, as can be seen from Figs. 15 and 16, where TCS for the ground and metastable states are presented.

IV. CONCLUSION

In the present study we have investigated the effects of the Debye-Hückel potential on the electron-hydrogen collision

processes using the CCC method. The effects of such a potential on the bound-state wave functions dramatically affect the excitation and ionization collision processes over the full incident-electron energy range. The TCS decrease with a decrease of Debye length, which is consistent with reduction of projectile-atom interaction as screening increases. Similarly, we find that with the reduction of Debye length D the excitation integrated CS decrease in magnitude, have a sharper rise at threshold, and have a broadening of the cross-section maximum. The TICS increases with increase of screening, which is the result of a large transfer of flux from the discrete spectrum to the continuum.

We hope that the calculated cross sections available via the CCC database [28] will be helpful for modeling Debye plasma transport and spectroscopy. In the future we are planning to include the Debye screening in the study of electron-helium scattering [31].

ACKNOWLEDGMENTS

This work was supported, in part, by the Australian Research Council and Curtin University. Resources of the Australian National Computational Infrastructure (NCI) Facility and its Western Australian node iVEC are gratefully acknowledged.

[1] M. S. Pindzola, S. D. Loch, J. Colgan, and C. J. Fontes, Phys. Rev. A **77**, 062707 (2008).
[2] P. Beiersdorfer, Phys. Scr. T **134**, 014010 (2009).
[3] Y. Y. Qi, J. G. Wang, and R. K. Janev, Phys. Rev. A **78**, 062511 (2008).
[4] L. Zhang and P. Winkler, Int. J. Quantum Chem. **60**, 1643 (1996).
[5] S. Kar and Y. K. Ho, J. Quant. Spectrosc. Radiat. Transfer **109**, 445 (2008).
[6] S. Lorenzen, A. Wierling, H. Reinholz, and G. Ropke, Contrib. Plasma Phys. **48**, 657 (2008).
[7] S. Lorenzen, A. Wierling, H. Reinholz, G. Ropke, M. C. Zammit, D. V. Fursa, and I. Bray, AIP Conf. Proc. **1290**, 99 (2010).
[8] A. Sil, S. Canuto, and P. Mukherjee, Adv. Quantum Chem. **58**, 115 (2009).
[9] D. Salzman, *Atomic Physics in Hot Plasmas*, 1st ed. (Oxford University Press, Oxford, 1998).
[10] S. B. Zhang, J. G. Wang, and R. K. Janev, Phys. Rev. Lett. **104**, 023203 (2010).
[11] S. B. Zhang, J. G. Wang, and R. K. Janev, Phys. Rev. A **81**, 032707 (2010).
[12] Y. Y. Qi, J. G. Wang, and R. K. Janev, Phys. Rev. A **80**, 032502 (2009).
[13] F. J. Rogers, H. C. Graboske, and D. J. Harwood, Phys. Rev. A **1**, 1577 (1970).
[14] B. Saha, P. K. Mukherjee, and G. H. F. Diercksen, Astron. Astrophys. **396**, 337 (2002).
[15] A. Ghoshal and Y. K. Ho, J. Phys. B **43**, 045203 (2010).
[16] Y. Y. Qi, Y. Wu, J. G. Wang, and Y. Z. Qu, Phys. Plasmas **16**, 023502 (2009).
[17] G. J. Hatton, N. F. Lane, and J. C. Weisheit, J. Phys. B **14**, 4879 (1981).
[18] Y. Jung and J. Yoon, J. Phys. B **29**, 3549 (1996).
[19] S. Kar and Y. K. Ho, Phys. Rev. E **70**, 066411 (2004).
[20] S. Kar and Y. K. Ho, New J. Phys. **7**, 141 (2005).
[21] S. Kar and Y. K. Ho, Few-Body Syst. **40**, 13 (2006).
[22] I. Bray and A. T. Stelbovics, Phys. Rev. Lett. **69**, 53 (1992).
[23] I. Bray and A. T. Stelbovics, Phys. Rev. A **46**, 6995 (1992).
[24] I. Bray and A. T. Stelbovics, Phys. Rev. Lett. **70**, 746 (1993).
[25] K. Bartschat and I. Bray, J. Phys. B **29**, L271 (1996).
[26] I. J. Thompson and A. R. Barnett, Comput. Phys. Commun. **36**, 363 (1985).
[27] K. Bartschat, I. Bray, P. G. Burke, and M. P. Scott, J. Phys. B **29**, 5493 (1996).
[28] I. Bray, Y. Ralchenko, K. Lewis, and ITP Group Curtin University, *CCC database* (2009), [http://atom.curtin.edu.au/CCC-WWW].
[29] M. B. Shah, D. S. Elliot, and H. B. Gilbody, J. Phys. B **20**, 3501 (1987).
[30] P. Defrance, W. Claeys, A. Cornet, and G. Poulaert, J. Phys. B **14**, 111 (1981).
[31] D. V. Fursa and I. Bray, Phys. Rev. A **52**, 1279 (1995).